DOI: 10.1002/ejic.200700753

Crystal and Magnetic Structure of Sr_2MReO_6 (M = Ni, Co, Zn) Double Perovskites: A Neutron Diffraction Study

María Retuerto,*[a] María Jesús Martínez-Lope,[a] Mar García-Hernández,[a] María Teresa Fernández-Díaz,[b] and José Antonio Alonso[a]

Keywords: Perovskite phases / Rhenium / Neutron diffraction / Crystal structure / Magnetic structure / Antiferromagnetism

A study of the crystallographic and magnetic structures of the oxides Sr_2MReO_6 (M = Ni, Co, Zn) was carried out on polycrystalline samples by using neutron powder diffraction (NPD) data. At room temperature the perovskite crystal structure is tetragonal, space group $I4/m$, and contains an almost completely ordered array of the tilted MO_6 and ReO_6 octahedra. When the temperature is decreased, Sr_2CoReO_6 and Sr_2ZnReO_6 undergo a phase transition to a monoclinic symmetry ($P2_1/n$ space group). The low-temperature magnetic structures, which were determined by NPD, show antiferromagnetic behavior for Sr_2NiReO_6 and Sr_2CoReO_6. For Sr_2NiReO_6, a antiferromagnetic structure was observed below T_N = 30 K, which was characterized by a propagation vector of k = (1/2, 0, 1/2); this structure remains stable down to 2 K and shows an ordered magnetic moment of 1.3(5) μ_B for the Ni^{2+} ions. Sr_2CoReO_6 is an antiferromagnet below T_N = 60 K and down to 2 K; the magnetic structure is defined by a propagation vector k = (0, 0, 1/2) and an ordered magnetic moment of 2.75(7) μ_B is refined for the Co^{2+} cations at 2 K. For Sr_2ZnReO_6, the magnetic measurements suggest the existence of an ordered magnetic array of Re^{6+} ($5d^1$) spins, which cannot be observed by NPD data.

Introduction

Double perovskites of the general formula $A_2BB'O_6$ (A = divalent cation or rare earth; B, B′ = transition metals) have been proposed as candidates for real applications in the field of spintronics. The interest in these compounds was renewed upon the report of half-metallic properties in Sr_2FeMoO_6, with the conduction band completely polarized.[1,2] This material presents magnetoresistance (MR) at room temperature; therefore, the electronic transport can be influenced by the application of an external magnetic field.[3] It is reported that the analogous double perovskite Sr_2FeReO_6 displays similar properties.[4,5] The crystal structure of these double perovskites is well known; it consists of a regular arrangement of corner-sharing BO_6 and $B'O_6$ octahedra alternating along the three directions of the crystal and the large A cations occupy the voids between the octahedra. Depending on the relative size of the B and B′ cations with respect to the A ion, the crystal structure has been defined either as cubic ($Fm3m$), tetragonal ($I4/m$), or monoclinic ($P2_1/n$).

The magnetic structure of these oxides can be described as an ordered arrangement of parallel Fe^{3+}($3d^5$, S = 5/2) magnetic moments that are antiferromagnetically coupled with Mo^{5+} ($4d^1$, S = 1/2) spins or Re^{5+} ($5d^2$, S = 1). It was proposed[6] that the magnetic interactions are mediated by itinerant electrons in the π*-bands coming from t_{2g} orbitals of Mo or Re ions. It was claimed that Re-based double perovskites present, in general, high magnetic ordering temperatures, as Re^{5+} cations have one more electron in the conduction band than Mo ions. For instance, Sr_2CrReO_6 has the highest T_C of 635 K[7] among the perovskite-like oxides and Ca_2FeReO_6 has a high T_C of 540 K.[8]

Concerning other reported Re-containing double perovskites, Sleight et al.[9,10] initially described Ba_2MReO_6 oxides, and they detailed their structural and magnetic properties. Afterward, much more research was carried out to understand the properties of these compounds.[3,11,12] Kato and coworkers[13] reviewed the Sr_2MReO_6 perovskites with M = Mg, Sc, Cr, Mn, Fe, Co, Ni, and Zn, and they showed a huge variety of magnetic and transport properties. The aim of this paper is to describe a more detailed neutron diffraction structural study of the Sr_2MReO_6 (M = Ni, Co, Zn) double perovskites. The main goal of this paper is the determination of their magnetic structures, in complement with magnetic susceptibility and magnetization data, including the report of a phase transition at low temperatures.

Results and Discussion

Crystallographic Structures

Sr_2MReO_6 (M = Ni, Co, Zn) oxides were obtained as black well-crystallized powders. The XRD diagrams at

[a] Instituto de Ciencia de Materiales de Madrid, CSIC, Cantoblanco, 28049 Madrid, Spain
[b] Institut Max Von Laue Paul Langevin, 38042 Grenoble, France

room temperature are characteristic of perovskite structures; in all cases, the double-perovskite patterns can be indexed in a tetragonal unit cell in the *I*4/*m* space group. As shown in Figure 1, the patterns show superstructure reflections corresponding to the long-range M/Re ordering [e.g., (011) and (013)]. The refinement of the M/Re occupancy factors allowed us to determine the cationic ordering over the B positions of the perovskite by Rietveld analysis of the XRD data (Figure 1); a 100% order was obtained for Sr_2NiReO_6 and Sr_2ZnReO_6 and a 98% order for Sr_2CoReO_6.

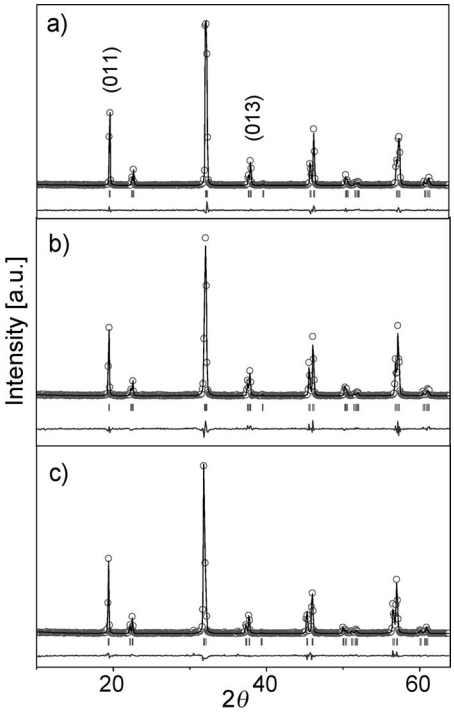

Figure 1. Observed (circles), calculated (full line), and difference (bottom) profiles of the XRD Rietveld refinements for the Sr_2MReO_6 oxides [M = Ni (a), Co (b), Zn (c)] showing the first two superstructure peaks related to M/Re ordering indexed in a tetragonal *I*4/*m* unit cell.

The reduction of the cubic symmetry to tetragonal, orthorhombic, or monoclinic symmetry as a result of the progressive tilting of the BO_6 octahedra involves small shifts in the positions of the oxygen atoms, which can be suitably detected by neutron diffraction. This tilting is due to a decrease in the Goldschmidt tolerance factor defined as $t = (A–O)/\sqrt{2}(B–O)$, when the A cation decreases or the B cations increase in average size.

The crystal-structure refinement was performed from high-resolution NPD data collected at room temperature with a wavelength $\lambda = 1.594$ Å in a tetragonal unit cell (space group *I*4/*m*). A structural model was defined with two crystallographically independent B positions (M and Re) and two kinds of nonequivalent oxygen atoms (O1 and O2). Sr_2NiReO_6 contains 0.57% of NiO as an impurity and it was refined as a second phase in the NPD pattern. The Sr_2CoReO_6 refinement gives an excellent fit for the room-temperature crystal structure. In a first trial, the tetragonal model for Sr_2ZnReO_6 gave a reasonable Bragg R factor of ≈8%, which was further improved with the introduction of a minor monoclinic $P2_1/n$ phase with the same composition and tightly related unit-cell parameters. This refinement, including 2.63% of the monoclinic phase, yielded a reduction in the Bragg factor of the main tetragonal phase to 6%, mainly concerning some high-angle regions of the diagram. This result suggests that Sr_2ZnReO_6 is, at room temperature, at the onset of a phase transition to a lower monoclinic symmetry, as reported by Kato et al.[13] who described 15% of a monoclinic phase at room temperature. The details of the monoclinic phase are given below when the low-temperature structures are discussed. The final refinement also included, as a third phase, vanadium metal from the sample holder. Figure 2 illustrates the good agreement between the observed and calculated high-resolution NPD patterns at room temperature for the three samples. The degree of M/Re order found from NPD data, by refinement of the metal occupancy factors, is similar to that previously determined from XRD data.

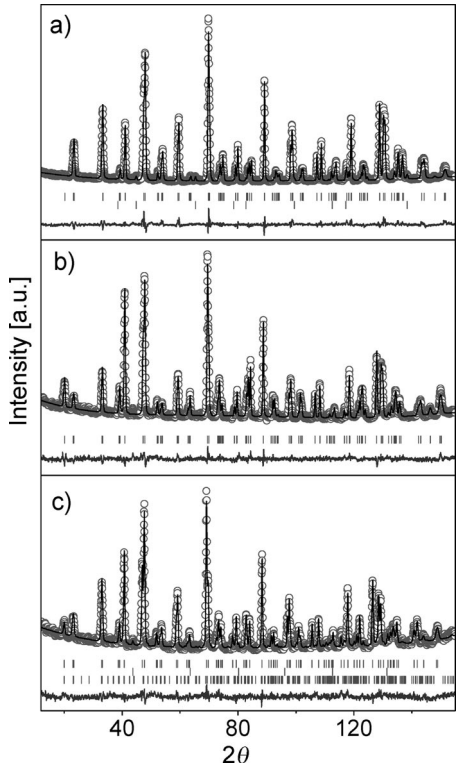

Figure 2. Observed (circles), calculated (full line), and difference (bottom line) NPD patterns corresponding to the refinement of (a) Sr_2NiReO_6, (b) Sr_2CoReO_6, and (c) Sr_2ZnReO_6 at room temperature.

Table 1 includes the atomic coordinates, lattice parameters, and volume at room temperature as well as the reliability factors after the structural refinement from NPD data. Table 2 contains the main interatomic distances and some selected bond angles.

Table 1. Atomic parameters and agreement factors after a Rietveld refinement of NPD data for Sr_2MReO_6 (M = Ni, Co, Zn) in the *I*4/*m* space group at room temperature.

	Ni	Co	Zn
*I*4/*m*			
a [Å]	5.54520(7)	5.5631(1)	5.5785(1)
b [Å]	5.54520(7)	5.5631(1)	5.5785(1)
c [Å]	7.9179(1)	7.9516(2)	8.0053(2)
V [Å^3]	243.471(6)	246.090(8)	249.127(8)
Sr 4d (0 1/2 1/4)			
B [Å^2]	0.72(2)	0.89(3)	1.05(4)
M 2a(0 0 0)			
B [Å^2]	0.27(7)	1.3(2)	0.9(1)
Re 2b (0 0 1/2)			
B [Å^2]	0.38(8)	0.07(4)	0.02(7)
O1 4e (0 0 *z*)			
z	0.2571(9)	0.2575(5)	0.2570(8)
B [Å^2]	0.94(4)	1.16(4)	1.28(5)
O2 8h (*x y* 0)			
x	0.2861(6)	0.2897(4)	0.2934(7)
y	0.2277(6)	0.2282(4)	0.2238(6)
B [Å^2]	0.75(2)	1.05(4)	1.19(5)
Reliability factors			
χ^2	0.896	0.576	0.507
R_p	4.34	3.26	3.89
R_{wp}	5.51	4.16	4.89
R_I	5.82	5.48	6.05

Table 2. Main bond lengths for MO_6 and ReO_6 octahedra [Å], selected angles [°] determined from NPD data at room temperature, and the bond-valence sums.

	Sr_2NiReO_6	Sr_2CoReO_6	Sr_2ZnReO_6
MO_6 octahedra			
M–O_1 (*x* 2)	2.036(7)	2.047(4)	2.053(7)
M–O_2 (*x* 4)	2.028(3)	2.051(2)	2.045(4)
M–O	2.032	2.049	2.049
ReO_6 octahedra			
Re–O_1 (*x* 2)	1.923(7)	1.928(4)	1.949(7)
Re–O_2 (*x* 4)	1.920(3)	1.912(2)	1.937(4)
Re–O	1.921	1.920	1.943
Angles around O			
Re–O_1–M	180.0	180.0	180.0
Re–O_2–M	166.6(1)	165.97(9)	164.44(2)
Re–O–M	173.3	173.0	172.2
Bond-valence sum (V_i)			
M	2.16	2.28	2.36
Re	5.82	5.84	5.48

The observed bond lengths M–O (Table 2), 2.032, 2.049, and 2.049 Å for Ni, Co, and Zn, respectively, are in all cases smaller than those expected from the sums of ionic radii[14] for $^{VI}Ni^{2+}$ (2.09 Å), $^{VI}Co^{2+}$ (2.145 Å), and $^{VI}Zn^{2+}$ (2.14 Å). The average Re–O bond lengths range from 1.920 (M = C_o) to 1.943 Å (M = Zn) and are also smaller than the expected value for Re^{6+}–O (1.95 Å). The same observation for M and Re distances at room temperature was reported by Kato et al.[13]

The calculation of the bond-valence sums allowed us to have an estimation of the oxidation states of the Re and M cations. The bond-valence sum (V_i) is calculated as $V_i = \Sigma_j S_{ij}$, where S_{ij} is the bond-valence between the *i*th and *j*th atoms, and it is defined as $S_{ij} = \exp[(d_0-d_{ij})/0.37]$,[15] where d_{ij} is the bond length between the *i*th and *j*th atoms and d_0 is the bond valence parameter. The d_0 parameters for Ni, Co, and Zn cations are 1.654, 1.692, and 1.704 Å, respectively; as for Re, we used d_0 = 1.91 Å as suggested by Kato et al.[13] The calculated valences, shown in Table 2, clearly suggest that Re is hexavalent and Ni, Co, and Zn are present in a divalent oxidation state.

At room temperature, the tetragonal superstructure of perovskite arises from the antiphase rotation of the oxygen octahedra with respect to the *c* axis ($a^0a^0c^-$ in Glazer's notation[16]). The superexchange Re–O–M bond angles decrease from Ni to Co to Zn, which is indicative of the higher degree of tilting in the ZnO_6 octahedra and the reduction of the symmetry. The magnitude of the octahedral tilting angles can be derived from the average bond angles as $\phi = (180 - \theta)/2$, where θ = M–O2–Re, to yield 6.7 (Ni), 7.0 (Co), and 7.8° (Zn).

Detailed inspection of the temperature-dependent NPD patterns collected at D20 clearly shows that the structural transition from tetragonal to monoclinic symmetries for Sr_2CoReO_6 occurs at around 90 K: new reflections indicating a reduction in symmetry are observed as the temperature is decreased. As an illustration, Figure 3 shows the thermal evolution of the intensity of the overlapping monoclinic [120] and [210] peaks, which is forbidden for the tetragonal symmetry. The NPD thermal evolution from 2 to 250 K of Sr_2ZnReO_6 shows the presence of a monoclinic phase over the entire temperature range, which suggests that the structural transition occurs above 250 K. This observation agrees with the presence of a minor monoclinic phase at room temperature as described above. The reduction in the symmetry found for the Co and Zn samples is a result of the smaller tolerance factor due to the larger ionic size of Co^{2+} and Zn^{2+} cations.

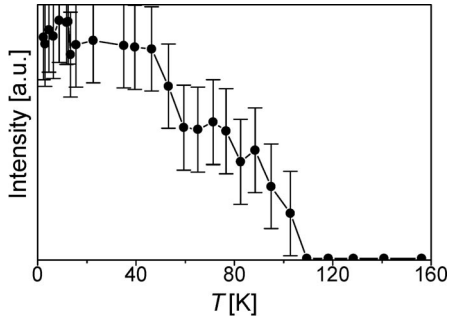

Figure 3. Thermal evolution of [120] monoclinic reflection in Sr_2CoReO_6.

Figure 4 shows a close-up of a section of the NPD diagrams at 2 K of Sr_2CoReO_6 and Sr_2ZnReO_6, initially refined in *I*4/*m*, which display a poor fit to the splitting of certain reflections; the fit was substantially improved by using the $P2_1/n$ space group, which models the splitting well. This space group contains two different positions for M and Re and three kinds of nonequivalent oxygen atoms (O1, O2, and O3), all in general (*x*, *y*, *z*) positions. The

monoclinic β angle is very close to 90°, which is thus indicative of a strong pseudoorthorhombic character of the unit cell. This symmetry and space group is adopted by other related and well-known double perovskites such as Sr_2FeWO_6,[17] Ca_2FeMoO_6,[18] or Nd_2MgTiO_6[19] with small tolerance factors. Table 3 contains the atomic coordinates, lattice parameters, volume, and reliability factors obtained after the final refinement of the NPD patterns at 2 K.

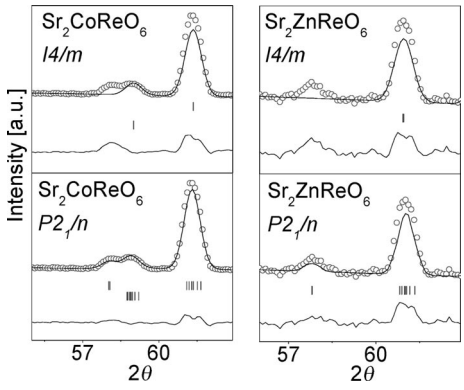

Figure 4. Observed (crosses), calculated (full line), and difference (bottom) NPD Rietveld profiles of Sr_2CoReO_6 and Sr_2ZnReO_6 at 2 K. The two sets of tick marks in the Sr_2CoReO_6 sample correspond to the crystallographic and magnetic structures. Upper and lower figures compare the refinements in the *I*4/*m* and $P2_1/n$ space groups, respectively.

Table 3. Atomic parameters and agreement factors after a Rietveld refinement of NPD data for Sr_2MReO_6 (M = Ni, Co, Zn) at 2 K.

	Ni		Co	Zn
*I*4/*m*		$P2_1/n$		
a [Å]	5.5024(4)	*a* [Å]	5.578(1)	5.614(1)
b [Å]	5.5024(4)	*b* [Å]	5.551(1)	5.5813(8)
c [Å]	7.9607(6)	*c* [Å]	7.865(2)	7.887(1)
V [Å^3]	241.02(3)	*V* [Å^3]	243.5(1)	247.14(8)
Sr 4d (0 1/2 1/4)		Sr 4e (*x y z*)		
B [Å^2]	0.302(1)	*x*	0.981(3)	0.993(3)
		y	0.011(3)	0.016(2)
		z	0.259(2)	0.257(3)
		B [Å^2]	–0.21(7)	–0.03(8)
M 2a (0 0 0)		M 2d (1/2 0 1/4)		
B [Å^2]	0.305(1)	*B* [Å^2]	–0.21(7)	–0.03(8)
Mag. mom. [μ_B]	1.3(5)	Mag. mom. [μ_B]	2.75(7)	0
Re 2b (0 0 1/2)		Re 2b (1/2 0 0)		
B [Å^2]	0.303(1)	*B* [Å^2]	–0.21(7)	–0.03(8)
O1 4e (0 0 *z*)		O1 4e (*x y z*)		
z	0.261(1)	*x*	0.054(3)	0.056(2)
B [Å^2]	0.18(6)	*y*	0.498(3)	0.496(3)
		z	0.271(4)	0.265(3)
		B [Å^2]	0.20(9)	0.13(9)
O2 8h (*x y* 0)		O2 4e (*x y z*)		
x	0.302(1)	*x*	0.735(4)	0.720(3)
y	0.228(1)	*y*	0.244(6)	0.247(4)
B [Å^2]	0.18(6)	*z*	0.014(8)	0.017(3)
		B [Å^2]	0.20(9)	0.13(9)
		O3 4e (*x y z*)		
		x	0.221(4)	0.230(4)
		y	0.213(4)	0.204(4)
		z	0.985(6)	0.970(3)
		B [Å^2]	0.20(9)	0.13(9)
Reliability factors				
χ^2	6.62	χ^2	25.2	1.90
R_p [%]	1.76	R_p [%]	0.957	1.01
R_{wp} [%]	2.48	R_{wp} [%]	1.48	1.37
R_I [%]	0.96	R_I [%]	0.30	1.00
$R_{mag.}$ [%]	23.2	$R_{mag.}$ [%]	7.5	0

At 2 K, the perovskite structure for Sr_2CoReO_6 and Sr_2ZnReO_6 contains alternating MO_6 and ReO_6 octahedra. The structures display in-phase octahedra tilting along the (001) direction of the pseudocubic cell and an antiphase along the (100) and (010) directions, which corresponds to the $a^-a^-b^+$ Glazer's notation as derived by Woodward[20] for 1:1 ordering in double perovskites, consistent with space group $P2_1/n$. The ABO_3 perovskite structures undergo usual bending of the B–O–B bonds upon cooling and, as a result, a slight monoclinic distortion is induced in the members of the series exhibiting a larger tilting angle at room temperature, Sr_2CoReO_6 and Sr_2ZnReO_6.

Magnetic Measurements

The temperature dependence of the susceptibility for Sr_2NiReO_6, measured under zero-field-cooled (ZFC) and field-cooled (FC) conditions, is presented in Figure 5a. For temperatures below $T \approx 20$ K, we observed thermomagnetic irreversibility between the ZFC and FC curves, which suggests a cluster glass-like behavior. The divergence in the FC and ZFC data was reported before in analogous perovskite-type compounds and was attributed to the formation of spin-glass or cluster-glass states.[21] This behavior is believed to arise due to the competition between different magnetic interactions, which hinder the establishment of a long-range ordered magnetic arrangement. Immediately above the convergence of the ZFC and FC curves, a small but significant peak in the susceptibility curve suggests the onset of an antiferromagnetic transition at $T_N = 25$ K. This anomaly cannot be ascribed to the minor NiO impurity (≈ 0.5%), as its Néel temperature is 550 K.

The inverse of the susceptibility presents a linear behavior at high temperature. A Curie–Weiss fit above 160 K gives a value of the paramagnetic effective moment of 3.11 μ_B/f.u., which compares with that expected for *spin-only* Ni^{2+} ($S = 1$) and Re^{6+}($S = 1/2$) of 3.32 μ_B. The negative value of the experimental paramagnetic temperature (–33 K) indicates the presence of antiferromagnetic interactions.

The isothermal magnetization curve measured at 5 K (Figure 5b) shows the presence of a narrow hysteresis cycle. At 20 kOe the magnetic moment is close to saturation. The saturation magnetization is 0.88 μ_B/mol, the remnant magnetization is 0.68 μ_B/mol and the coercitive field is 2.2 kOe. A similar behavior is observed at 10 K, with a saturation magnetization of 0.68 μ_B/mol, a remnant magnetization of 0.51 μ_B/mol and the coercitive field of 0.57 kOe. However, the isotherm recorded at 22 K shows a distinct behavior, with a low-field linear region characteristic of an antiferromagnetic ordering that, above 6 kOe, presents a change in slope characteristic of a metamagnetic transition induced

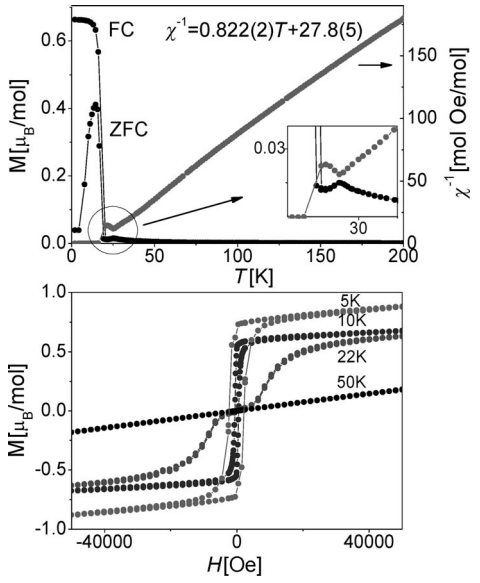

Figure 5. (a) Thermal evolution of the susceptibility (field cooling and zero-field cooling) and inverse of the susceptibility for Sr_2NiReO_6, (b) isothermal magnetization at T = 5, 10, 22, and 50 K.

by the magnetic field. Metamagnetic transitions occur in antiferromagnetic systems where the spontaneous antiferromagnetic interactions are weak in nature and the long-range antiferromagnetic structure can be destroyed by the application of an external magnetic field; they correspond to a spin-flop transition from an AF state to a spin ferromagnetically polarized state.[22] The 50 K isotherm corresponds to a paramagnetic system.

The thermal evolution of the susceptibility of Sr_2CoReO_6 is reported in Figure 6a. The susceptibility exhibits a low temperature maximum at T_N = 57 K that corresponds to the transition from the high temperature paramagnetic state to a low temperature antiferromagnetically ordered phase. The reciprocal susceptibility data above T_N shows a slight curvature, probably due to crystal field effects or a progressive change in the population on the low-spin versus High-spin electronic configurations of the Co ions.[23]

A Curie–Weiss fit above 200 K gives a paramagnetic effective moment of 4.88 μ_B/f.u. Considering the presence of high-spin Co^{2+}(S = 3/2), the total paramagnetic moment for the configuration $Co^{2+}(3d^7)$–$Re^{6+}(5d^1)$ would be 4.24 μ_B. The slightly larger effective moment could be explained if we suppose a partially unquenched orbital contribution of the high-spin Co^{2+}. Other double perovskites such as $Sr_3CoSb_2O_9$,[24] Sr_2CoWO_6,[25] Sr_2CoTeO_6, Ca_2CoTeO_6,[26] and Sr_2CoUO_6[27] show magnetic moment values for Co^{2+} in between 4.90 μ_B and 5.20 μ_B. These values are assigned to unquenched orbital magnetic contributions. The Weiss temperature of –140 K confirms the presence of antiferromagnetic interactions. The magnetization versus field is also characteristic of an antiferromagnetic system (Figure 6b). It is linear, which excludes the presence of any weak ferromagnetism effect.

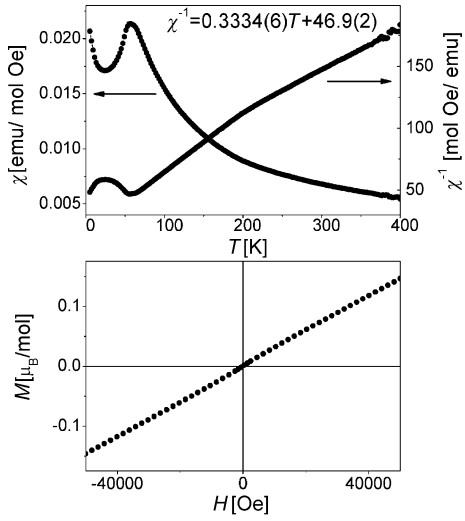

Figure 6. (a) Thermal variation of the susceptibility for Sr_2CoReO_6 and thermal evolution of the inverse of the susceptibility at H = 1000 Oe, (b) magnetization curve of Sr_2CoReO_6 at T = 5 K.

The variation of the magnetic susceptibility of Sr_2ZnReO_6 is shown in Figure 7. The reciprocal susceptibility shows a complex temperature dependence, with three inflection points at 10, 100, and 350 K. A tentative fit to a Curie–Weiss fit above 350 K gives a μ_{eff} of 0.83 μ_B and a Weiss temperature of 235 K, which implies the presence of ferromagnetic interactions between Re^{6+} ($5d^1$) cations. The 5 K isotherm also confirms the presence of weak ferromagnetic interactions and gives rise to a hysteresis cycle with a coercive field of 1.5 kOe; there is no saturation of the magnetization, which suggests the participation of antiferromagnetic interactions in this complex magnetic system.

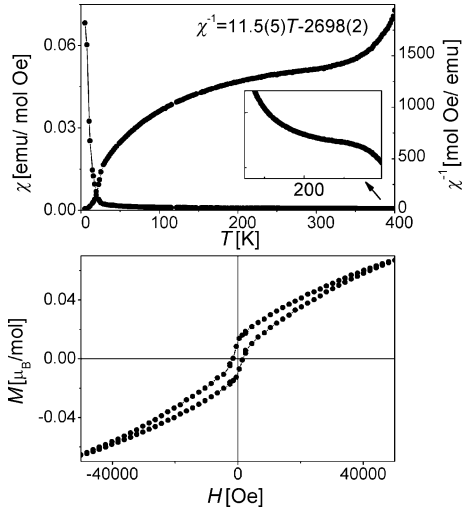

Figure 7. (a) The susceptibility and inverse of the susceptibility of Sr_2ZnReO_6 at H = 1000 Oe, (b) magnetization vs. field isotherm at 5 K.

Magnetic Structures

The thermal evolution of the NPD patterns collected between 2 and 250 K (λ = 2.42 Å) is shown in Figure 8. Sr_2Ni-

ReO_6 and Sr_2CoReO_6 present new reflections at positions forbidden for the crystallographic Bragg reflections; and Sr_2ZnReO_6 does not present any new magnetic diffraction peak or any magnetic contribution in an existing reflection.

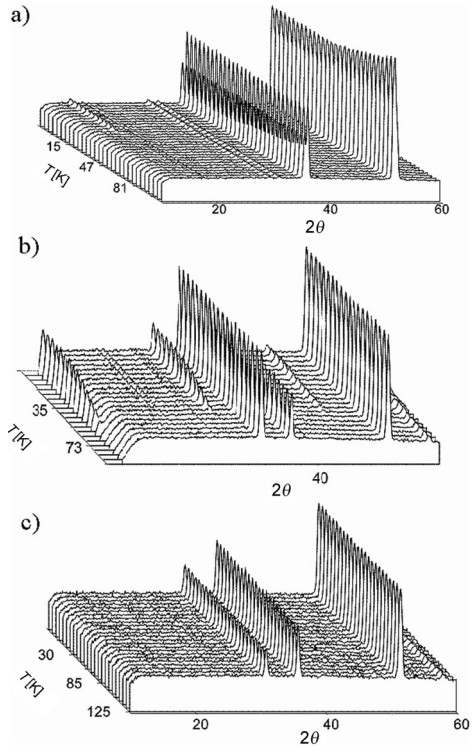

Figure 8. Thermal evolution of the NPD patterns of Sr_2MReO_6 [M = Ni (a), Co (b), Zn (c)] collected with λ = 2.42 Å.

Sr_2NiReO_6 shows very weak new reflections appearing at positions forbidden for the space group *I*4/*m* (Figure 8a). The magnetic peaks are indexed with the propagation vector k = (1/2,0,1/2). The two magnetic Ni atoms present in the unit cell, Ni1 at (000) and Ni2 at (1/2,1/2,1/2) are magnetically coupled as $m_{1x} = -m_{2x}$, $m_{1y} = -m_{2y}$, and $m_{1z} = -m_{2z}$. This magnetic arrangement leads to good agreement between the observed and calculated magnetic intensities. A trial refinement with magnetic moments over the Re sites gave no improvement to the magnetic fit; the Re moments converge to negligible values with large standard deviations. The final refinement only included magnetic moments on the Ni positions. Figure 9a shows the final Rietveld plot including three phases: the crystallographic phase, the magnetic phase, and the NiO impurity. A view of the magnetic structure is displayed in Figure 10a. It can be described as an antiferromagnetic stacking of ferromagnetic [1 0 1] planes. This magnetic arrangement is also observed in other double perovskites such as Sr_2NiMoO_6[28] or Ba_2FeWO_6.[29] Figure 11a shows the thermal variation of the Ni ordered magnetic moment, with large error bars due to the small intensity of the magnetic reflections. At 2 K the magnetic moment over the Ni sites is 1.3(5) μ_B. The Néel temperature, where the magnetic peak vanishes, is 30 K, in good agreement with that determined from susceptibility measurements (Figure 5a). It is important to remark that the NPD technique was not able to detect the apparent ferromagnetic ordering suggested by the increase in the magnetization in the FC curve below 20 K for Sr_2NiReO_6. This result confirms that this susceptibility anomaly is not accompanied by long-range ferromagnetic ordering of the Ni spins. As discussed before, the large divergence between ZFC and FC curves suggests the presence of a cluster-glass state, lacking from the long-range coherence required to give rise to an extra contribution in the low-temperature NPD patterns. The mentioned divergence may be a symptom of a considerable degree of magnetic frustration, which could be related to the anomalous thermal behavior of the *c* unit cell parameter, as it will be discussed below.

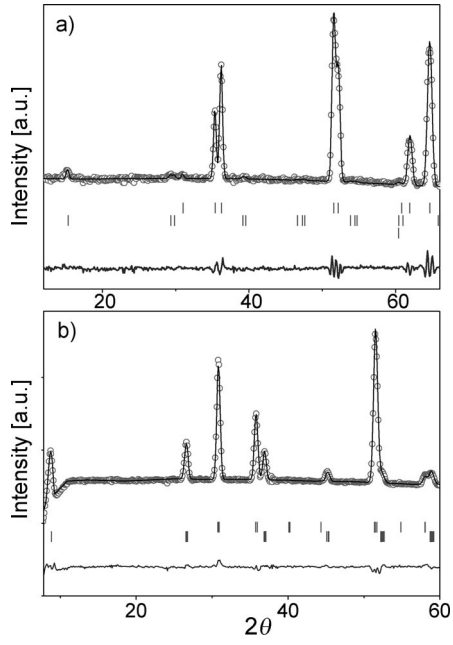

Figure 9. Rietveld fit from NPD data for (a) Sr_2NiReO_6 and (b) Sr_2CoReO_6 oxides. Observed (circles), calculated (full line), and difference (bottom) profiles at 2 K.

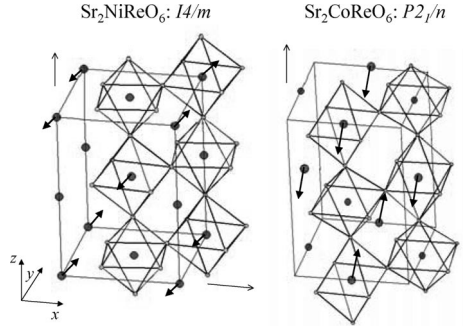

Figure 10. (a) Magnetic structure of Sr_2NiReO_6 with the magnetic moments plotted on the Ni atoms, the structure is tetragonal and k = (1/2, 0, 1/2), (b) magnetic structure of Sr_2CoReO_6 with the magnetic moments plotted on the Co atoms, the structure is monoclinic and k = (0, 0, 1/2).

For Sr_2CoReO_6 the magnetic diffraction peaks were observed at temperatures below 60 K (Figure 8b). These new peaks are forbidden for the crystallographic Bragg reflec-

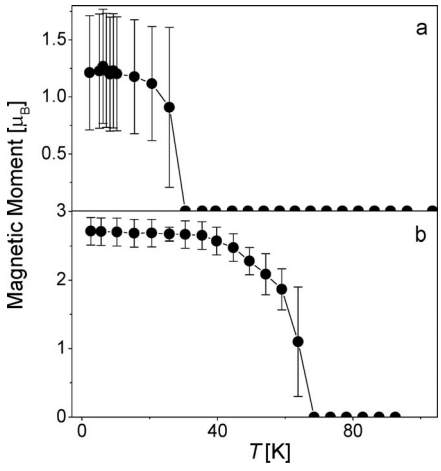

Figure 11. Thermal variation of the magnetic moments of (a) Ni and (b) Co in Sr_2MReO_6 (M = Ni, Co).

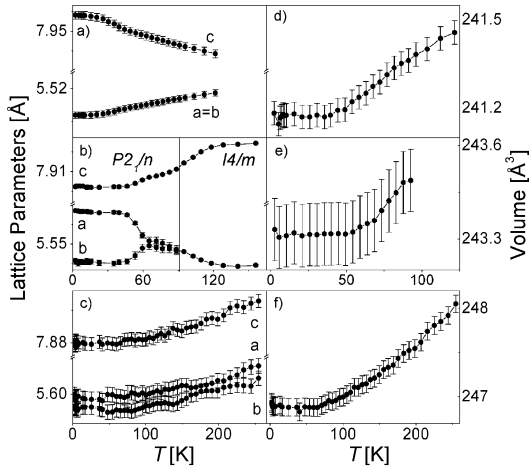

Figure 12. Thermal evolution of the lattice parameters of (a) Sr_2NiReO_6, (b) Sr_2CoReO_6, (c) Sr_2ZnReO_6 and the volume of (d) Sr_2NiReO_6, (e) Sr_2CoReO_6, (f) Sr_2ZnReO_6.

tions in the space group $P2_1/n$. The peaks correspond to magnetic satellites defined by the propagation vector k = (0, 0, 1/2). The two magnetic Co atoms of the unit cell, Co1 at (1/2,0,1/2) and Co2 at (0,1/2,0) are magnetically coupled as $m_{1x} = -m_{2x}$, $m_{1y} = -m_{2y}$, and $m_{1z} = -m_{2z}$. We do not consider the magnetic moment over the Re sites due to their negligible values after a trial refinement. Figure 9b shows the final Rietveld plot including the crystallographic phase and the magnetic phase. The collinear magnetic structure is shown in Figure 10b. It can be described as an antiferromagnetic array along c of ferromagnetic [0 0 1] planes. The Co spins are approximately directed along the [0 1 1] direction. The thermal evolution of the magnetic moments is displayed in Figure 11b; the ordered magnetic moment on the Co atoms at 2 K is 2.75(7) μ_B, which is close to the expected moment for high-spin Co^{2+} cations (3 μ_B). The observed onset of magnetic ordering, at 60 K, is similar to the observed maximum in magnetic susceptibility at 57 K.

No magnetic contribution was observed on the low-temperature NPD patterns for Sr_2ZnReO_6 (Figure 8c); the small magnetic moment observed in the 5 K magnetization isotherm (Figure 7b) is clearly below the detection threshold for neutron diffraction.

Figure 12a illustrates the thermal variation of the lattice parameters of Sr_2NiReO_6, Sr_2CoReO_6, and Sr_2ZnReO_6. Upon warming, Sr_2NiReO_6 exhibits a progressive reduction in the tetragonal distortion (a/c ratio) as it is expected; surprisingly, the c parameter presents an unusual contraction as temperature increases, which is probably due to a large degree of spin-lattice coupling. Moreover, the volume has a nonexpected behavior and remains almost constant below T_N; above T_N, the usual thermal expansion of the cell is observed (Figure 12d). This effect is again a symptom of magnetic frustration upon the establishment of the ordered magnetic structure.[30]

The structural transition of Sr_2CoReO_6 at 90 K is obvious in the evolution of the unit cell parameters (Figure 12b). The sample also presents an anomalous behavior coincident with the establishment of the magnetic ordering at T_N = 60 K; upon cooling c abruptly decreases and a increases, whereas b remains approximately constant. As observed for the Ni compound, the cell volume (Figure 12e) remains constant below T_N, which can also be attributed to geometrical magnetic frustration. This magnetic structure intrinsically involves a high degree of frustration, as each Co moment is surrounded by four Co spins in a ferromagnetic arrangement, at distances of about 5.5 Å, and eight Co spins in an antiferromagnetic array, at the same distances.

It is remarkable that Sr_2ZnReO_6 presents a similar behavior in the evolution of the volume at low temperatures (Figure 12f) that roughly coincides with the inflection observed in the susceptibility at about 100 K. This is indicative of long-range magnetic ordering of Re^{6+} ($5d^1$) magnetic moments, although the small magnitude of the ordered moments at the Re sites prevents the observation of the magnetic structure by NPD techniques.

Conclusions

Three Re-based double perovskites of composition Sr_2MReO_6 (M = Ni, Co, Zn) were prepared by soft chemistry methods. The crystal structure at room temperature is defined in a tetragonal unit cell (space group $I4/m$); the crystal contains alternating MO_6 and ReO_6 octahedra tilted in antiphase along the c axis. At low temperature, Sr_2CoReO_6 and Sr_2ZnReO_6 undergo a reduction in symmetry to monoclinic ($P2_1/n$). For M = Ni, the magnetic measurements display a complex behavior; below 20 K, the presence of a strong irreversibility is ascribed to the formation of a cluster-glass system; at 22 K a metamagnetic transition is observed, switching from an antiferromagnetic structure to a spin-polarized arrangement promoted by an external magnetic field. The main novelty of this investigation is the report of the magnetic structures of Sr_2NiReO_6 and Sr_2CoReO_6, studied from NPD data, in which we observed a different arrangement of the Ni^{2+} ad Co^{2+} spins. For Sr_2Ni-

ReO_6, it is defined by a propagation vector k = (1/2, 0, 1/2) below 30 K and it consists of ferromagnetic [1 0 1] layers of collinear Ni moments coupled antiferromagnetically, whereas for Sr_2CoReO_6, it is defined by k = (0, 0, 1/2) below 60 K, containing ferromagnetic layers coupled antiferromagnetically along the c axis. The magnetic properties and the unit-cell variation of Sr_2ZnReO_6 also suggest the existence of an ordered array of Re^{6+} ($5d^1$) spins, although the small magnitude of the ordered moments at Re sites prevents the observation of the magnetic structure from the NPD data.

Experimental Section

Sr_2MReO_6 (M = Ni, Co, Zn) oxides were prepared in polycrystalline form by a soft chemistry procedure designed to obtain very reactive precursors. Stoichiometric amounts of $Sr(NO_3)_2$, Re metal, and $Ni(NO_3)_2{\cdot}6H_2O$, $Co(NO_3)_2{\cdot}6H_2O$, or ZnO were dissolved in an aqueous citric acid solution containing a few drops of nitric acid to favor the dissolution of Re metal. The citrate and nitrate solutions were slowly evaporated leading to organic resins containing a homogeneous distribution of the involved cations. The resins were dried at 120 °C and then decomposed at 600 °C in air, with elimination of the organic materials and nitrates. This treatment gave rise to homogeneous precursor materials. Then, the samples were treated at 1200 °C for 12 h in a N_2 inert flow.

The samples were first characterized by X-ray diffraction (XRD) in Bragg–Brentano reflection geometry with Cu-K_α radiation (λ = 1.5418 Å). Neutron powder diffraction (NPD) experiments were carried out at ILL, Grenoble, France, in the high-resolution powder diffractometer D2B (λ = 1.594 Å) at room temperature and in the high-flux diffractometer D20 (λ = 2.4197 Å) in a range of temperatures between 2 and 250 K. The refinement of the crystal and magnetic structures was performed by the Rietveld method by using the FULLPROF refinement program.[31] A pseudo-Voigt function was chosen to generate the line shape of the diffraction peaks. The scale factor, background coefficients, zero-point error, pseudo-Voigt corrected for asymmetry parameters, positional coordinates, isotropic thermal factors, and occupancy factors for oxygen atoms were refined in the final run. For the low temperature data sets collected in D20, the x, y, and z components of the magnetic moments localized on the transition-metal ions were also refined.

The magnetic susceptibilities were measured with a commercial SQUID magnetometer on powdered samples under a 0.1-T magnetic field in the temperature range 5–400 K. The isothermal magnetization curves were obtained for magnetic fields going from –5 to 5 T.

Acknowledgments

We thank the financial support of CICyT to the projects MAT2004–0479 and MAT2005–06024-C02–01 and we are grateful to ILL for making all facilities available.

[1] K. I. Kobayashi, T. Kimura, H. Sawada, K. Terakura, Y. Tokura, *Nature* **1998**, *395*, 677.
[2] T. H. Kim, M. Uehara, S. W. Cheong, S. Lee, *Appl. Phys. Lett.* **1999**, *74*, 1737.
[3] Y. Tomioka, T. Okuda, Y. Okimoto, R. Kumain, K. I. Kobayashi, *Phys. Rev. B* **2000**, *61*, 422.
[4] K. I. Kobayashi, T. Kimura, Y. Tomioka, H. Sawada, K. Terakura, *Phys. Rev. B* **1999**, *59*, 11159.
[5] Z. Fang, K. Terakura, J. Kanamori, *Phys. Rev. B* **2001**, *63*, 180407.
[6] D. D. Sarma, Priya Mahadevan, T. Saha-Dasgupta, Sugata Ray, Ashwani Kumar, *Phys. Rev. Lett.* **2000**, *85*, 2549.
[7] H. Kato, T. Okuda, Y. Okimoto, Y. Tomioka, Y. Takenoya, A. Ohkubo, M. Kawasaki, Y. Tokura, *Appl. Phys. Lett.* **2002**, *81*, 328.
[8] W. Westerburg, O. Lang, C. Ritter, C. Felser, W. Tremel, G. Jakob, *Solid State Commun.* **2002**, *122*, 201.
[9] A. W. Sleight, J. Longo, R. Ward, *Inorg. Chem.* **1962**, *1*, 245.
[10] A. W. Sleight, J. F. Weiher, *J. Phys. Chem. Solids* **1972**, *33*, 679.
[11] T. Alamelu, U. V. Varadaraju, M. Venkatesan, A. P. Douvalis, J. M. D. Coey, *J. Appl. Phys.* **2002**, *91*, 8909.
[12] A. Poddar, S. Das, *Z. Phys. B, Condens. Matter Quanta* **2004**, *344*, 325.
[13] H. Kato, T. Okuda, Y. Okimoto, Y. Tomioka, K. Oikawa, T. Kamiyama, Y. Tokura, *Phys. Rev. B* **2004**, *69*, 184412.
[14] R. D. Shannon, *Acta Crystallogr., Sect. A* **1976**, *32*, 751.
[15] N. E. Brese, M. O'Keefe, *Acta Crystallogr., Sect. B* **1991**, *47*, 192.
[16] A. M. Glazer, *Acta Crystallogr., Sect. B* **1972**, *28*, 3384.
[17] D. Sanchez, J. A. Alonso, M. Garcia-Hernandez, M. J. Martínez-Lope, M. T. Casais, *J. Phys.: Condens. Matter* **2005**, *17*, 3673.
[18] J. A. Alonso, M. T. Casais, M. J. Martínez-Lope, J. L. Martínez, P. Velasco, A. Muñoz, M. T. Fernández-Díaz, *Chem. Mater.* **2000**, *12*, 161.
[19] W. A. Groen, F. P. F. Van Berkel, D. J. W. IJdo, *Acta Crystallogr., Sect. C* **1986**, *42*, 1472.
[20] P. M. Woodward, *Acta Crystallogr., Sect. B* **1997**, *53*, 32.
[21] R. Rodriguez, A. Fernandez, A. Isalgue, J. Rodriguez, A. Labrata, J. Tejada, X. Obradors, *J. Phys. C* **1985**, *18*, L401.
[22] R. S. Perry, L. M. Galvin, S. A. Grigera, L. Capogna, A. J. Schofield, A. P. Mackenzie, M. Chiao, S. R. Julian, S. I. Ikeda, S. Nakatsuji, Y. Maeno, C. Pfleiderer, *Phys. Rev. Lett.* **2001**, *86*, 2661.
[23] M. J. Martínez-Lope, J. A. Alonso, M. T. Casais, M. T. Fernández-Díaz, *Eur. J. Inorg. Chem.* **2002**, 2463.
[24] V. Primo-Martín, M. Jansen, *J. Solid State Chem.* **2001**, *157*, 76.
[25] M. C. Viola, M. J. Martínez-Lope, J. A. Alonso, J. L. Martínez, J. M. De Paoli, S. Pagola, J. C. Pedregosa, M. T. Fernández-Díaz, R. E. Carbonio, *Chem. Mater.* **2003**, *15*, 1655.
[26] M. S. Augsburger, M. C. Viola, J. C. Pedregosa, A. Muñoz, J. A. Alonso, R. E. Carbonio, *J. Mater. Chem.* **2005**, *15*, 993.
[27] R. Pinacca, M. C. Viola, J. C. Pedregosa, A. Muñoz, J. A. Alonso, J. L. Martínez, R. E. Carbonio, *Dalton Trans.* **2005**, 447.
[28] M. J. Martinez-Lope, J. A. Alonso, M. T. Casais, *Eur. J. Inorg. Chem.* **2003**, *15*, 2839.
[29] A. K. Azad, S.-G. Eriksson, A. Mellergard, S. A. Ivanov, J. Eriksen, H. Rundlöf, *Mater. Res. Bull.* **2002**, *37*, 1797.
[30] J.-W. G. Bos, J. P. Attfield, *Phys. Rev. B* **2004**, *70*, 174434.
[31] J. Rodriguez-Carvajal, *Physica B (Amsterdam)* **1993**, *192*, 55.

Received: July 16, 2007
Published Online: November 28, 2007

